C. R. Chimie 19 (2016) 1597–1604

Contents lists available at ScienceDirect

Comptes Rendus Chimie

www.sciencedirect.com

Full paper/Mémoire

Duration of JJ stent in situ is critical: An ultrastructural and mechanical investigation

Effet de la durée de séjour in situ sur les propriétés des sondes JJ: une étude par MEB et par analyse mécanique

Christophe Poulard [a, *], Arnaud Dessombz [a, b], Michel Daudon [c, d], Dominique Bazin [a, e]

[a] *Laboratoire de Physique des Solides, Université Paris-Sud, CNRS, UMR 8502, 91405 Orsay cedex, France*
[b] *INSERM, UMR 1138, Centre de Recherche des Cordeliers, Laboratoire de Physiopathologie, Orale Moléculaire, Équipe Berdal, 15, rue de l'École-de-Médecine, 75006 Paris, France*
[c] *Sorbonne Universités, UPMC (Université Paris-6), UMR S 702, 75005 Paris, France*
[d] *APHP, Service des Explorations Fonctionnelles, Hôpital Tenon, 75020 Paris, France*
[e] *Sorbonne Universités, UPMC (Université Paris-6), CNRS, Collège de France, Laboratoire de Chimie de la Matière Condensée de Paris (LCMCP), 11, place Marcelin-Berthelot, 75005 Paris, France*

ARTICLE INFO

Article history:
Received 29 July 2015
Received in revised form 3 October 2016
Accepted 3 October 2016
Available online 10 November 2016

Keywords:
JJ stents
Urology
Surface defect
Chemical analysis
SEM observation
Mechanical analysis

ABSTRACT

The JJ stent constitutes a medical device extensively used nowadays by urologists in more than 40,000 patients per year in France. In this investigation, we characterize the surface state and the elastic properties of a set of JJ stents on which pathological calcifications are present. These encrustations have been identified by Fourier transform infrared spectroscopy. A surface examination by scanning electron microscopy indicates the existence of defects. The striking point of these observations is that black marks, present at the surface to help urologists during the operation, significantly alter the surface and may serve as nucleation centers. Moreover, elastic properties are not preserved when the indwelling time of JJ stents is longer than 12 wk. Such data may help industrial companies to develop new JJ stents, which avoid the formation of encrustations and help the clinician to optimize the lifetime of JJ stents in patients.

Mots-clés:
Sondes JJ
Urologie
Défaut de surface
Analyse FTIR
Observation MEB
Analyse mécanique

RÉSUMÉ

Les sondes JJ constituent un dispositif médical largement utilisé de nos jours par les urologues chez plus de 40 000 patients par an en France. Dans cette étude, nous caractérisons l'état de surface et les propriétés élastiques d'un ensemble de sondes JJ sur lesquelles des calcifications pathologiques sont présentes. Ces incrustations ont été identifiées par spectrophotométrie infrarouge à transformée de Fourier. Un examen de surface par microscopie électronique à balayage indique l'existence de défauts. Le point marquant de ces observations vient du fait que les marques noires présentes à la surface pour aider les urologues pendant l'opération modifient de manière significative la surface et peuvent

* Corresponding author.
E-mail address: christophe.poulard@u-psud.fr (C. Poulard).

http://dx.doi.org/10.1016/j.crci.2016.10.002

servir de sites de nucléation. De plus, les propriétés élastiques ne sont pas conservées lorsque le temps de séjour de ces sondes chez le patient est supérieur à 12 semaines. Ces données peuvent donc aider les industriels à développer de nouvelles sondes JJ évitant la formation d'incrustations et aider le clinicien à optimiser la durée de vie des sondes JJ chez les patients.

1. Introduction

To ensure drainage of urine from the kidney into the bladder, a stent, name proposed in 1973 by Dr. J. Montie, is placed in the urinary tract. In 1978, Dr. R.P. Finney introduced the “double-J” ureteral stent design, which is curled at both the top and bottom [1]. Usually inserted with the aid of a cystoscope [2], in length it varies between 24 and 30 cm (for adults), and more than 40,000 patients in France benefit from such devices each year.

There are several causes of urinary tract obstruction, but the most common are stone disease [3,4], junction syndrome, and extrinsic compression from nonurologic neoplasms. Several investigations have been focused on interactions between JJ stents and kidney stone concretions [5,6] in humans [7–11] as well as in animals [12]. Because of the presence of incrustations, it is sometimes impossible to withdraw or replace the stent over a guide [13,14]. Moreover, the ability of the stent to prevent duct collapse depends on its compression strength, which decreases as degradation progresses [15]. Thus, as emphasized by several studies [16,17], stent encrustation constitutes a serious complication of ureteral stent use, especially in stone formers. Importantly, Bithelis et al. [18] observed that the mean mass of encrustation in stone formers was larger (71.05 mg) than that in patients without stones (1 mg).

Among the materials used in JJ stents [19–23] are polyurethane [24,25], silicone [26,27], and metallic alloy [28–32]. The coefficient of friction as well as irritation and cell adhesion at the biomaterial–tissue interface [33,34] of stents can be reduced by coatings [35,36]. The aim of this investigation is to assess the physicochemical integrity of JJ stents on which calcifications are present. To this end, the characterization techniques [37–39], Fourier transform infrared spectroscopy (FTIR) [40,41] and field effect scanning electron microscopy (FE-SEM) [42], have been used. These have already been successful in determining the chemical composition of biological concretions (see for example Ref. [43]) and describing mesoscopic topology [44]. As clearly shown by Pariente and Conort [45], SEM can be used to visualize the surface of JJ stents. In this article, we also report the uniaxial traction test to evaluate elasticity properties (Young's modulus) of the JJ stents [46].

2. Materials and methods

All 68 JJ stents analyzed in the present study were from Tenon Hospital. We followed the usual procedures. All participants gave their verbal consent, documented by the researchers, for use of the material. Samples were examined without knowledge of the patient's name or other identifying data. Ethical approval was obtained from the ethics committee of Tenon Hospital. The investigation conformed to the principles of the Declaration of Helsinki.

All concretions on the JJ stents were characterized by FTIR (Vector 22; Bruker Spectrospin, Wissembourg, France) according to a previously defined analytical procedure [47,48]. Data were collected in the absorption mode between 4000 and 400 cm^{-1} with a resolution of 4 cm^{-1}.

An FEI/Philips XL40 environmental FE scanning electron microscope was used for characterization at the mesoscopic scale. Such an environmental scanning electron microscope can image nonconductive materials without any conductive coating and thus permits direct observation with no damage to biological samples. Imaging was performed with a gaseous secondary electron detector, with an accelerating voltage of 20 kV and a water pressure of 0.4 Torr (53.3 Pa) in the chamber.

The mechanical properties were analyzed by uniaxial traction (Adamel Lhomargy DY-30) by placing a millimetric part of the JJ stent between two steel clamping jaws. The initial distance between the two jaws and, hence the initial length of the JJ stent are noted as L_0. A hard cylinder with a diameter equal to the internal diameter of the stent was previously inserted at both ends to prevent their compression between the jaws. The displacement is imposed by the operator, and the force F was sampled every 50 ms by a force sensor up to 1 kN. The initial section S of the stent is evaluated through the measurement of the external and internal diameters of the JJ stent with an optical microscope. For elastomers, the elastic modulus E (Young's modulus) should be analyzed using the neo-Hookean model described by

$$\sigma = \frac{E}{3}\left(\lambda - \frac{1}{\lambda^2}\right) \quad (1)$$

where $\sigma = F/S$ is the stress, $\lambda = L/L_0$ is the elongation, but other mechanical properties should be analyzed in terms of stress σ and strain $\varepsilon = \lambda - 1$.

To compare the mechanical properties of the stents and the amount of crystal deposits, we established an incrustation score as described in Table 1.

Statistical comparisons relating mechanical parameters, indwelling time, and the chemical content of encrustations were performed using the Mann–Whitney test, multivariate analysis of variance, or chi-square test, when appropriate, with the NCSS statistical package (J. Hintz, Gainesville, FL). A P value of less than 0.05 was considered as statistically significant.

Table 1
Scale for scoring encrustations on ureteral double-J stents.

Score	Definition
0	No mineral encrustation, no biofilm
1	Few crystals, or small, well-circumscribed plaques of fine organic encrustation, especially at stent orifices
2	Some crystals, or more or less extensive plaques of the fine organic film
3	Fairly numerous locally confluent mineral encrustations, or a fine organic film covering part of the outer and inner surface of stent, and clogging some orifices within this section
4	Many confluent, but thin, mineral encrustations, or an extensive organic film covering part of outer and inner surface of the stent, and nearly completely clogging orifices within this section
5	Extensive mineral encrustations, thick in places (1 mm), surrounding part of stent, or an extensive organic film covering part of the outer and inner surfaces, clogging several orifices, and even partially or completely occluding the lumen
6	Stone formed at the end or on body of stent

3. Results and discussion

Morphological aspects at the macroscopic and mesoscopic scale

Table 2 presents the data for 16 JJ stents examined first by FTIR and FE-SEM for characterization of encrustations.

On the macroscopic scale, encrustations may be present in the middle (Fig. 1a) and at the curves (Fig. 1b) of JJ stents (red arrows). Continuous immersion of JJ stents in urine means that encrustations are usually present on the bottom curve. In a previous study, the inner and outer surfaces of the stents were examined under optical microscopy to detect the presence of a biofilm and/or mineral encrustations [16,49]. Encrustations (taken along the stents either by scraping with a scalpel or by using a needle under optical microscopy) were scored on a 0–6 scale (Table 2).

Observations at the mesoscopic scale give supplementary information on the chemistry of these pathological calcifications. For example, Fig. 1c shows typical cystine crystallites exhibiting flat surfaces with well-defined corners and edges, a result consistent with the hexagonal structure of cystine [50–52]. At this point, we introduce the terms nanocrystals and crystallites as defined by Van Meerssche and Feneau-Dupont [53] to describe the hierarchical structure of these pathological concretions. Crystallites (measuring typically some tens of micrometers) are made up of a collection of nanocrystals (measuring typically some hundreds of nanometers).

Similar observations with respect to crystallites of struvite (Fig. 1d) [54–56] and calcium oxalate dihydrate or weddellite (Fig. 1e) can be made. In Fig. 1f, we can observe bacterial imprints on layers of apatitic calcium phosphate [57,58]. We have previously proposed such an approach in cases of negative urine culture results to highlight the presence of bacteria that may contribute to stone formation.

Fig. 2 shows different kinds of structural defects at the surface of JJ stents. Some of them are probably because of manipulations when these devices are positioned between the kidney and the bladder (Fig. 2a and b). In Fig. 2c, it seems that part of the coating is absent. In Fig. 2d, a defect in holes in the JJ stent has clearly played a key role in the formation of the encrustation.

To highlight the major role of surface defects in the occurrence of encrustations, we have compared a macroscopic observation (Fig. 2e), in which white deposits on the black marks on the surface of JJ stents (blue arrow on Fig. 1a) are visible, and microscopic observations of these same marks (Fig. 2f). Importantly, note the high surface roughness of the marks. It seems that this step in the fabrication of the stents significantly modifies the surface, leading to a significant nidus for encrustation.

Finally, Fig. 2g shows an encrustation, which follows the linear defects present at the surface of a JJ stent.

Table 2
Selection of biological data corresponding to the 16 different JJ stents selected for this investigation, observed through FE-SEM and FTIR.

JJ stents	Sex, age[a]	Pathology	Indwelling time (d)	Encrustation code[b]	Composition (%) of encrustations as given by FTIR spectroscopy[c]
60643	F, 76	Lithiasis	57	1K-6B	MAP 60 + AmUr 20 + CA 15 + PROT 5
60644	M, 59	Tumor	23	2K-3B	CA 60 + ACCP 30 + PROT 10
60646	M, 54	Lithiasis	56	3K-4B	COM 85 + PROT 15
60648	M, 41	Lithiasis	131	3K-6B	COD 73 + Br 10 + COM 10 + PROT 5 + OCP 2
60649	M, 65	Tumor of ureter	28	2K-1B	COM 88 + PROT 7 + TRG 5
60653	M, 68	Lithiasis	76	3K-2B	PROT 85 + MPS 10 + COM 5
60654	F, 46	Tumor	113	3K-3B	PROT 75 + MPS 15 + COM 5 + COD 5
60655	M, 37	Lithiasis	82	2K-2B	CA 60 + MAP 30 + PROT 10
60656	M, 37	Lithiasis	125	2K-2B	MAP 50 + CA 25 + PROT 15 + COD 5 + COM 5
60693	M, 53	Hematuria	–	3K-3B	COM 50 + COD 35 + PROT 15
60694	M, 53	Hematuria	–	5K-2B	COM 80 + PROT 20
60698	F, 37	Lithiasis	129	1K-5B	CA 70 + AmUr 20 + PROT 10
60699	M, 71	Lithiasis	69	2K-3B	COM 45 + COD 45 + PROT 10
60700	M, 51	Lithiasis	–	4K-3B	CYS 90 + PROT 10
60701	M, 73	Lithiasis	–	6K-3B	COM 90 + PROT 10
60704	M, 69	Stenosis	73	1K-1B	COM 80 + PROT 15 + MPS 5

[a] Age is expressed in years.
[b] Range for encrustation score: 0–6 for kidney (K) and bladder (B).
[c] ACCP = amorphous carbonated calcium phosphate, AmUr = ammonium hydrogen urate, Br = brushite, CA = Ca phosphate apatite, COD = weddellite, COM = whewellite, CYS = cystine, MAP = struvite, MPS = mucopolysaccharides, OCP = octacalcium phosphate pentahydrate, PROT = proteins, TRG = triglycerides.

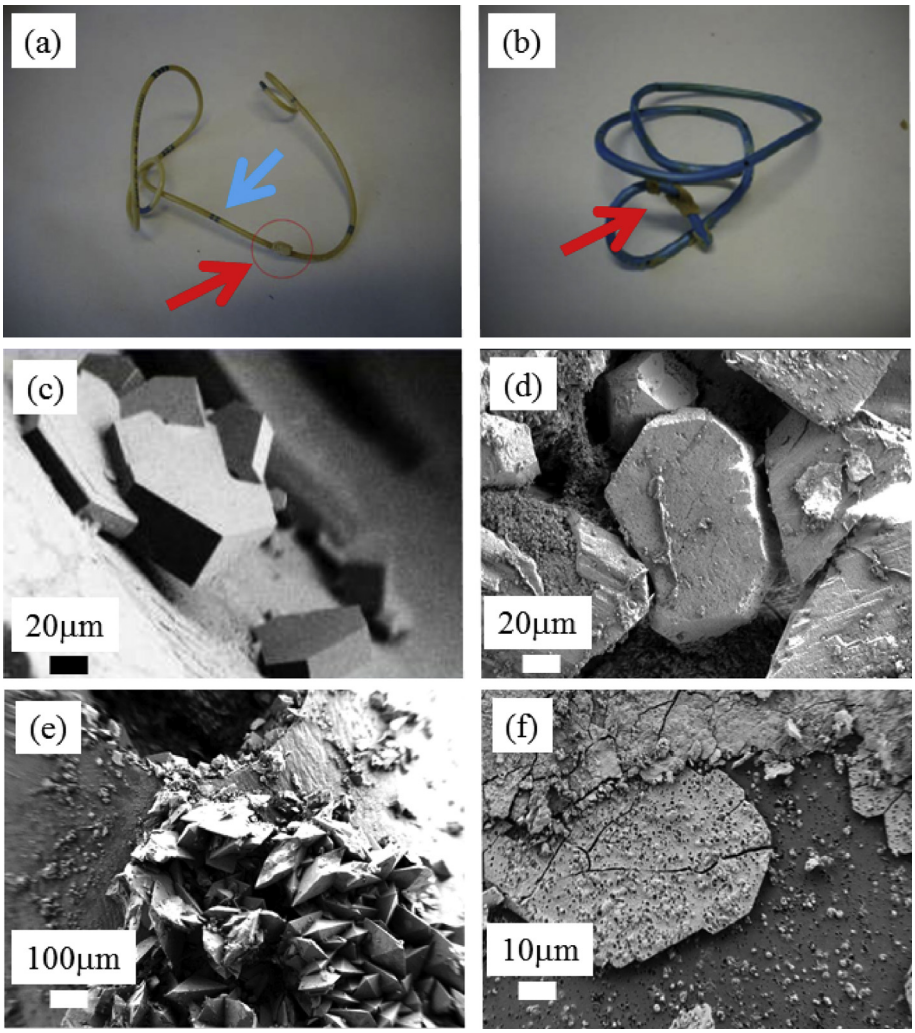

Fig. 1. (a and b) Typical encrustations present on JJ stents (red arrows). (c) Cystine crystallites present at the surface of JJ stents. (d) Agglomeration of struvite crystallites, (e) weddellite crystallites, and (f) bacterial imprints present on layers of Ca phosphate apatite.

Mechanical properties

As for the mechanical analysis, Fig. 3 shows the relationship between the stress and deformation, or the "λ-function." The two experiments shown in Fig. 3 were performed on the same stent (N57614) but in the presence (in red) or absence (in blue) of a hole.

The properties appear identical whether a hole is present or not, except for the maximal deformation ε_r tolerated by the stent before its rupture, which are 525 and 875%, respectively. This maximal deformation is always higher, in every case, in the absence of a hole. This can be readily understood by the fact that the presence of a hole on the stent causes a stress concentration area on its periphery that can weaken the material. The first phase, corresponding to elastic behavior of the stent, is exactly the same in this representation because the force is normalized, in the definition of stress, by the actual section of the stent. From this phase, we can extract the Young modulus, E, which is related to the slope of these curves by Eq. (1). We can also define the limit of elasticity, σ_l, which corresponds to the end of the elastic behavior and the beginning of the plastic phase where irreversible damage occurs in the material. In this typical experiment on a widely used stent, we notice that the limit of elasticity is not particularly high (close to 5 MPa), corresponding to a force close to 10 N, thus an applied mass of roughly 1 kg.

Table 3 presents all the data from the 52 JJ stents, which were investigated for their mechanical properties.

In Fig. 4, we have represented the evolution of the Young modulus and the limit of elasticity for different stent indwelling times, irrespective of pathology. The mean values for these two parameters were $\overline{E} = 12$ MPa and $\overline{\sigma} = 4.6$ MPa, respectively, that is, lower than the theoretical value of the unused stent ($E = 17.4$ MPa and $\sigma = 5.5$ MPa). Clearly, Young's modulus decreased with increasing indwelling time (slope, -0.021; $r^2 = 0.12$; $P = 0.0137$). A significant difference with respect to Young's modulus was

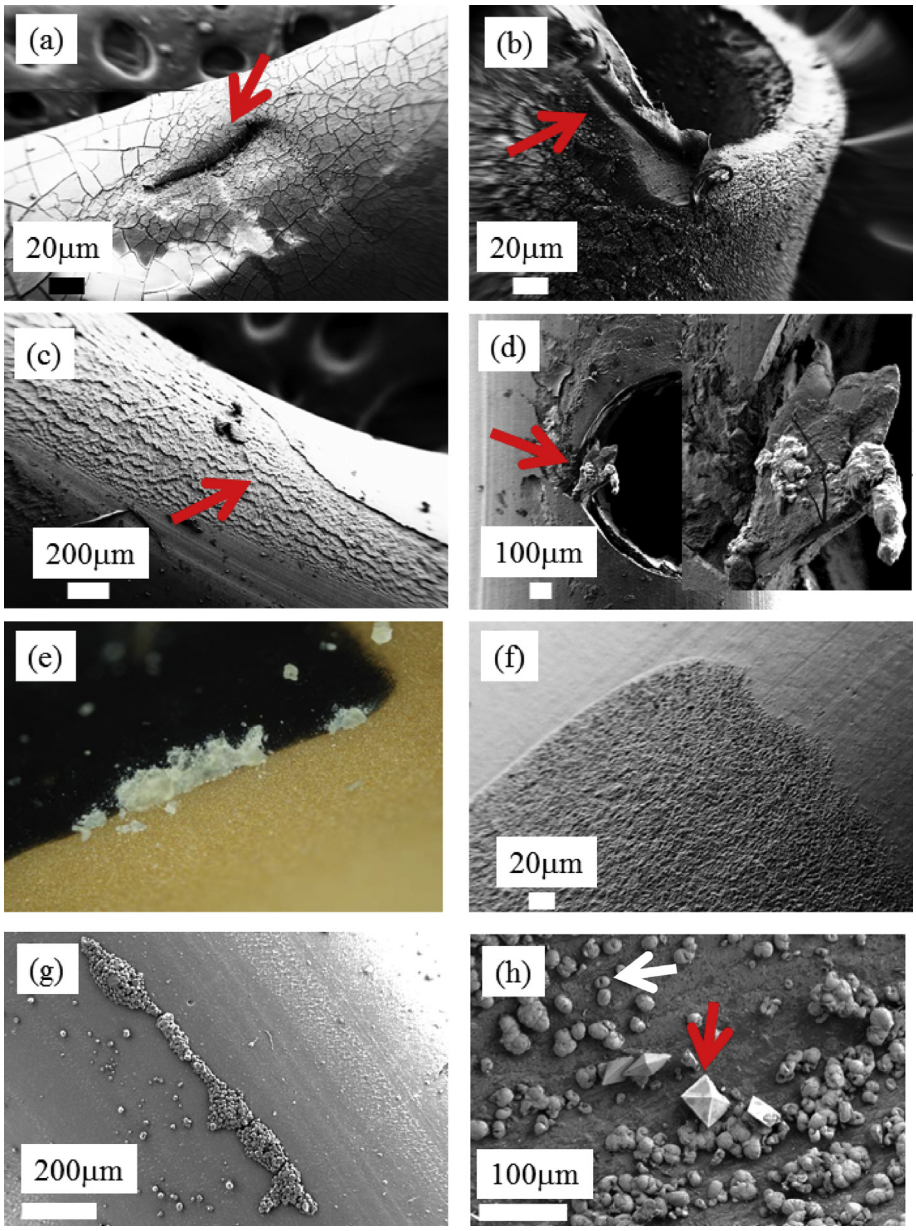

Fig. 2. (a–d) Examples of surface defects at the surface of JJ stents. (e) Macroscopic observations of JJ stent. (f) SEM observations of the black marks. (g) Spherical entities made of Ca phosphate apatite along a linear surface defaults. (h) Weddellite (red arrow) and whewellite (white arrow) crystallites coating the JJ stent surface.

found for an indwelling time greater than 12 wk relative to an indwelling time less than 3 wk (9.7 vs 12.6 MPa, $P = 0.03$). In contrast, the limit of elasticity remained unchanged with time ($P = 0.44$).

As expected, the encrustation score was time-dependent, the mean indwelling time increasing from 42.9 d for a score of 1 to 128.7 d for a score of 3 ($P = 0.03$). An exception was found for encrustations containing struvite, a marker of urinary tract infection because of bacterial urea catabolism. In such cases, the encrustation score was high (4 or 5) for an indwelling time around 47 d.

Interestingly, the limit of elasticity was influenced by the level of encrustation, increasing from 3.89 to 5.53 MPa when the encrustation score increased from 1 to 5 ($P = 0.0073$).

Fig. 5 represents the evolution with time of the relative deformation at rupture (deformation at rupture normalized by the deformation at rupture of the unused stent) for different stents with no hole between jaws. The mean value of this maximal deformation is 39% of that for an unused stent where no hole is present and reduces to 23% at a hole. The inset shows that the maximal

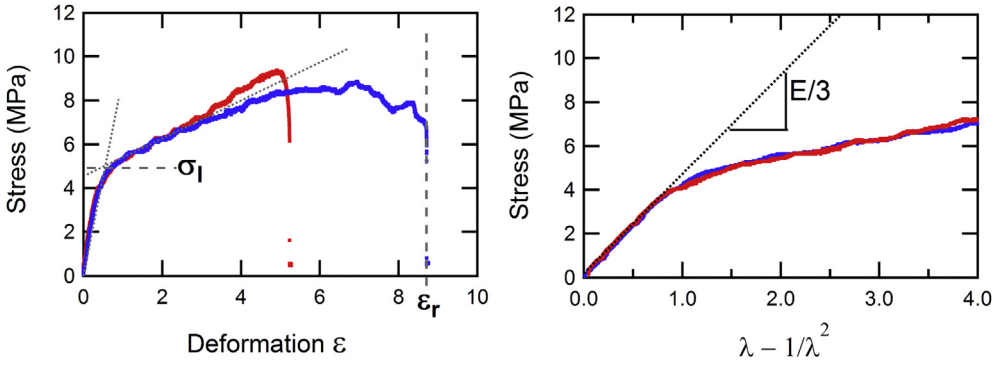

Fig. 3. Evolution of the stress (in MPa) measured on two parts of a stent (with or without a hole) vs the deformation ε (left) and the λ-function (right).

deformation for an unused stent is 2100%. The initial behavior of the probe is exactly the same except that it will rupture earlier. We can also notice that if the applied stress goes higher than 10 MPa the stent breaks immediately. The relative deformation at rupture is independent of indwelling time.

4. Conclusion and perspectives

This investigation has focused on JJ stents to assess their surface characteristics and their elastic properties. The complete data establish that several kinds of surface defects exist, probably related to manipulation and/or

Table 3
Selection of biological data corresponding to the 52 different stents used for mechanical analysis.

Stent	Sex, age[a]	Pathology	Indwelling time (d)	Encrustation code[b]	Composition (%) of encrustations as given by FTIR analysis[c]
N32782	M, 38	Lithiasis	25	3K-2B	COD 73 + PROT 12 + COM 10 + Br 3 + CA 2
N32998	M, 45	Lithiasis	73	2K-2B	COD 85 + PROT 10 + CA 5
N33213	F, 51	Tumor	55	1K-1B	COM 80 + PROT 15 + CA 5
N33220	F, 49	Tumor	96	2K-2B	AU2 60 + AU0 20 + COM 13 + PROT 5 + CA2
N33414	F, 75	Tumor	186	2K-2B	COM 85 + PROT 15
N33880	M, 30	Lithiasis	25	2K-1B	COM 80 + PROT 16 + CA 4
N42481	M, 30	Lithiasis	51	2K-6B	CYS 70 + PROT 20 + CA 10
N42894	M, 67	Lithiasis	81	1K-0B	PROT 50 + MPS 30 + COM 12 + COD 8
N42928	M, 47	Lithiasis	66	1K-3B	COD 75 + COM 15 + PROT 10
N43196	F, 51	Graft	38	2K-1B	PROT 80 + MPS 20
N43198	M, 72	Graft	60	0K-1B	PROT 75 + MPS 25
N43321	F, 22	Lithiasis	60	5K-5B	CA 40 + MAP 30 + ACCP 15 + AmUr 10 + PROT 5
N43329	M, 66	Lithiasis	9	1K-0B	PROT 85 + COM 15
N43362	M, 67	Lithiasis	45	1K-0B	PROT 45 + COM 25 + MPS 15 + CA 10 + ACCP 5
N43381	M, 40	Lithiasis	20	1K-1B	COM 60 + PROT 25-MPS 15
N43384	M, 34	Lithiasis	144	1K-0B	CA 60 + PROT 20 + COM 10 + COD 5 + AU2 5
N43386	F, 31	Lithiasis	47	1K-1B	COM 70 + PROT 25 + MPS 5
N43593	M, 57	Lithiasis	20	1K-1B	PROT 60 + MPS 30 + COM 10
N43596	M, 49	Tumor	150	1K-1B	PROT 75 + MPS 25
N43629	M, 50	Lithiasis	8	1K-1B	PROT 55 + COD 30 + MPS 15
N43632	F, 64	Lithiasis	54	2K-2B	COM 90 + PROT 10
N43651	M, 41	Lithiasis	18	1K-2B	COM 60 + PROT 20 + MPS 10 + COD 10
N43657	M, 30	Lithiasis	42	2K-1B	CYS 90 + PROT 10
N43659	M, 40	Lithiasis	42	5K-4B	COD 80 + PROT 15 + CA 5
N43665	M, 68	Lithiasis	75	2K-1B	CYS 80 + ACCP 10 + PROT 10
N43754	F, 76	Lithiasis	35	4K-4B	CA 60 + MAP 25 + ACCP 10 + PROT 5
N45258	M, 55	Lithiasis	15	1K-1B	COD 70 + PROT 20 + MPS 10
N45370	M, 47	Graft	45	2K-2B	AU0 40 + COM 30 + PROT 20 + MPS 10
N45371	M, 33	Tumor	41	2K-2B	COM 55 + MPS 30 + PROT 15
N45372	M, 66	Graft	20	1K-1B	PROT 50 + MPS 30 + COM 15 + COD 5
N45373	F, 25	Graft	18	1K-0B	PROT 50 + MPS 40 + COM 10
N45398	M, 23	Lithiasis	74	4K-5B	AU0 65 + AU2 20 + PROT 10 + COM 5
N45402	M, 31	Lithiasis	77	3K-4B	CYS 70 + PROT 20 + MPS 8 + CA 2
N45550	M, 39	Lithiasis	30	1K-2B	COM 50 + PROT 30 + MPS 20
N45552	M, 59	Lithiasis	225	2K-3B	COM 75 + PROT 25
N45663	F, 69	Lithiasis	10	2K-1B	COD 65 + COM 20 + PROT 15
N45664	F, 35	Graft	24	1K-1B	PROT 85 + MPS 15
N45799	M, 42	Lithiasis	45	1K-2B	COM 70 + PROT 20 + MPS 10
N45928	M, 72	Lithiasis	77	1K-0B	PROT 65 + COM 20 + MPS 15

Table 3 (*continued*)

Stent	Sex, age[a]	Pathology	Indwelling time (d)	Encrustation code[b]	Composition (%) of encrustations as given by FTIR analysis[c]
N57447	M, 67	Tumor	111	2K-3B	PROT 60 + MPS 20 + COM 15 + COD 5
N57482	M, 45	Lithiasis	63	1K-3B	COM 70 + COD 20 + PROT 10
N57561	M, 58	Lithiasis	62	2K-1B	COM 45 + COD 25 + PROT 15 + MPS 10 + CALC 5
N57614	F, 36	Lithiasis	53	3K-4B	COM 65 + COD 25 + PROT 10
N57780	F, 37	Lithiasis	65	2K-2B	CA 35 + COM 25 + COD 15 + PROT 15 + MPS 10
N57783	M, 28	Lithiasis	120	1K-2B	COM 45 + COD 30 + PROT 15 + MPS 10
N57786	M, 70	Tumor	91	2K-2B	COM 50 + COD 25 + PROT 15 + MPS 10
N59747	F, 26	Lithiasis	36	4K-4B	CA 50 + COM 35 + PROT 15
N59766	M, 62	Lithiasis	10	2K-2B	COM 60 + PROT 30 + CA 5 + MPS 5
N59768	M, 66	Lithiasis	28	3K-5B	MAP 45 + CA 35 + ACCP 10 + PROT 10
N59772	M, 60	Lithiasis	13	2K-2B	PROT 75 + MPS 15 + COM 10
N59783	M, 54	Lithiasis	26	3K-3B	COM 65 + PROT 35
N60361	M, 35	Lithiasis	24	1K-4B	CYS 80 + PROT 15 + COM 5

[a] Age is expressed in years.
[b] Range for encrustation score: 0–6 for kidney (K) and bladder (B).
[c] ACCP = amorphous carbonated calcium phosphate; AmUr = ammonium hydrogen urate; AU0 = anhydrous uric acid; AU2 = uric acid dihydrate; Br = brushite; CA = Ca phosphate apatite; CALC = calcite; COM = whewellite; COD = weddellite; CYS = cystine; MAP = struvite; MPS = mucopolysaccharides; PROT = proteins; TRG = triglycerides.

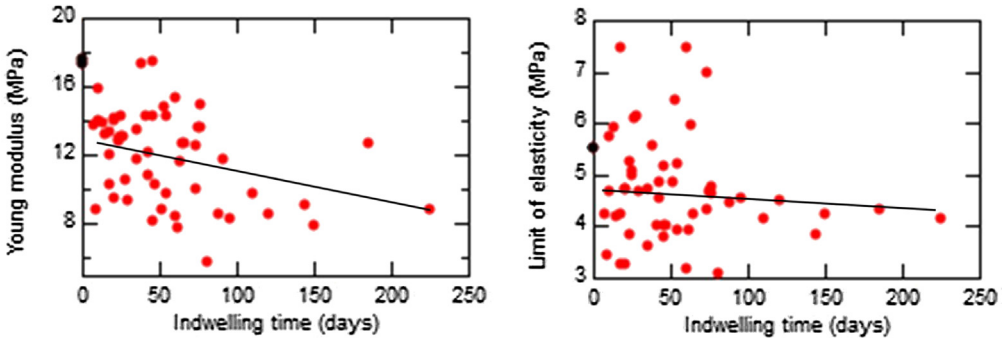

Fig. 4. Evolution of the Young modulus (left) and the limit of elasticity (right) vs the indwelling time of different stents (black, unused stent; red, used stents).

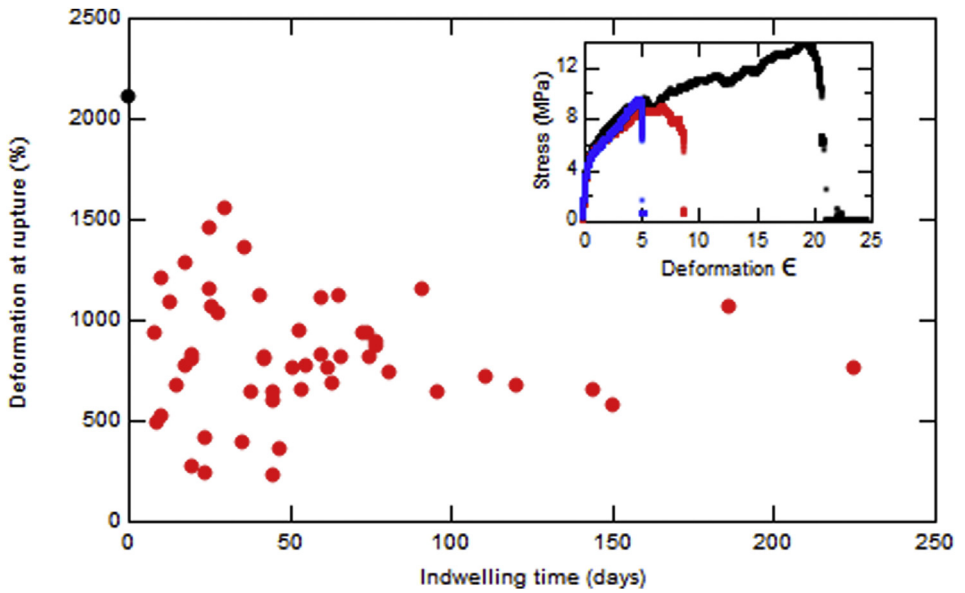

Fig. 5. Evolution of the maximal deformation before rupture vs the indwelling time of different stents with no hole. Inset: Evolution of stress with the deformation for an unused stent (black), a used stent without hole (red), and a used stent with hole (blue).

fabrication procedures. An important finding is that black marks on the surface of the stents, for the purpose of guiding the urologist during the medical procedure, correspond to very rough surfaces. Such roughness may favor the formation of encrustations. Regarding the elastic properties, this first set of measurements indicates that the mechanical strength is strongly reduced whatever the indwelling time and the presence of holes along the stent heightens this effect. This could be a serious problem when removing the stent, although no change is observed at the elastic phase.

JJ stents are currently in widespread use. As encrustations are a major limitation of such medical devices, we believe in approaches such as ours, combining studies of surface state with measurements of elastic properties, can be used to develop new devices and help to select better performance materials.

References

[1] R.P. Finney, J. Urol. 1 (1978) 120.
[2] J.W.H. Evans, D.J. Ralph, Br. J. Urol. 67 (1991) 109.
[3] S. Bariol, T. Farebrother, S. Ruthven, F. MacNeil, J. Endourol. 17 (2003) 741.
[4] F. Desgrandchamps, F. Moulinier, M. Daudon, P. Teillac, A. Le Duc, Br. J. Urol. 79 (1997) 24.
[5] D. Bazin, M. Daudon, C. Combes, C. Rey, Chem. Rev. 112 (2012) 5092.
[6] D. Bazin, M. Daudon, J. Phys. D: Appl. Phys. 45 (2012) 383001.
[7] E. Lechevallier, C. Saussine, O. Traxer, Prog. Urol. 18 (2008) 1024.
[8] S.P. Gorman, M.M. Tunney, J. Biomater. Appl. 12 (1997) 136.
[9] M.F. Bultitude, R.C. Tiptaft, J.M. Glass, P. Dasgupta, Urology 62 (2003) 622.
[10] B.A. Vanderbrink, A.R. Rastinehad, M.C. Ost, A.D. Smith, J. Endourol. 22 (2008) 905.
[11] M. Roumiguié, J.-B. Beauval, J. Guillotreau, B. Bordier, N. Doumerc, F. Sallusto, M. Mouzin, L. Bellec, M. Thoulouzan, P. Labarthe, P. Plante, M. Soulié, B. Malavaud, P. Rischmann, X. Gamé, Prog. Urol. 22 (2012) 701.
[12] M. Shafat, K. Rajakumar, H. Syme, N. Buchholz, M.M. Knight, Urolithiasis 41 (2013) 481.
[13] N.S.I. Gordon, Br. J. Urol. 64 (1989) 195.
[14] C. Eghazarian, E. Lechevallier, D. Bretheau, F. Jean, C. Coulange, Prog. Urol. 5 (1995) 410.
[15] S. Laaksovirta, T. Välimaa, T. Isotalo, P. Törmälä, M. Talja, T.L. Tammela, J. Urol. 170 (2003) 468.
[16] H. Bouzidi, O. Traxer, B. Doré, J. Amiel, H. Hadjadj, P. Conort, M. Daudon, Prog. Urol. 18 (2008) 230.
[17] M.M. Tunney, P.F. Keane, D.S. Jones, S.P. Gorman, Biomaterials 17 (1996) 1541.
[18] G. Bithelis, N. Bouropoulos, E.N. Liatsikos, P. Perimenis, P.G. Koutsoukos, G.A. Barbalias, J. Endourol. 18 (2004) 550.
[19] K. Al-Lamee, Med. Device Technol. 11 (2000) 20.
[20] D.T. Beiko, B.E. Knudsen, J.D. Denstedt, J. Endourol. 17 (2003) 195.
[21] E. Duguet, J.-L. Pariente, P. Conort, Prog. Urol. 15 (2005) 865.
[22] B.H. Chew, M. Duvdevani, J.D. Denstedt, Expert Rev. Med. Devices 3 (2006) 395.
[23] N. Venkatesan, S. Shroff, K. Jayachandran, M. Doble, J Endourol. 24 (2010) 191.
[24] S. Agrawal, C.T. Brown, E.A. Bellamy, R. Kulkarni, Br. J. Urol. Int. 103 (2008) 372.
[25] I. Singh, N.P. Gupta, A.K. Hemal, M. Aron, A. Seth, P.N. Dogra, Urology 58 (2001) 526.
[26] I. Singh, Indian J. Surg. 65 (2003) 405.
[27] J.W. Hoe, Australas. Radiol. 33 (1989) 385.
[28] M. Robert, A.M. Boularan, M. El Sandid, D. Grasset, Urol. Int. 58 (1997) 100.
[29] E.N. Liatsikos, D. Karnabatidis, K. Katsanos, P. Kallidonis, P. Katsakiori, G.C. Kagadis, N. Christeas, Z. Papathanassiou, P. Perimenis, D. Siablis, J. Urol. 182 (2009) 2613.
[30] A.A. Aown, K. Iason, K. Panagiotis, E.N. Liatsikos, Indian J. Urol. 26 (2010) 474.
[31] P. Sountoulides, A. Kaplan, O.G. Kaufmann, N. Sofikitis, Br. J. Urol. 105 (2010) 1066.
[32] P. Sountoulides, Indian J. Urol. 27 (2011) 305.
[33] J.W. Costerton, K.J. Cheng, G.G. Geesey, T.I. Ladd, J.C. Nickel, M. Dasgupta, T.J. Marrie, Annu. Rev. Microbiol. 41 (1987) 435.
[34] L. Cormio, P. La Forgia, A. Siitonen, M. Ruutu, Eur. Urol. 40 (2001) 354.
[35] J.D. Denstedt, in: A.P. Evan, J.E. Lingeman, J.C. Williams Jr. (Eds.), Renal Stone Disease. Am. Inst. Phys. Conf. Proc., Melville, NY, USA, 2007, p. 272.
[36] R. Bonniol, P. Meria, A. Safsaf, B. Albouy, L. Sibert, Prog. Urol. 21 (2011) 397.
[37] D. Bazin, M. Daudon, P. Chevallier, S. Rouzière, E. Elkaim, D. Thiaudiere, B. Fayard, E. Foy, P.A. Albouy, G. André, G. Matzen, E. Véron, Ann. Biol. Clin. 64 (2006) 125.
[38] D. Bazin, J.-P. Haymann, E. Letavernier, J. Rode, M. Daudon, Presse Med. 43 (2014) 135.
[39] D. Bazin, M. Daudon, Ann. Biol. Clin. 73 (2015) 517.
[40] M. Daudon, Feuill. Biol. 44 (2003) 19.
[41] M. Daudon, D. Bazin, J. Phys.: Conf. Ser. 425 (2013) 022006.
[42] F. Brisset, M. Repoux, J. Ruste, F. Grillon, F. Robaut, Microscopie électronique à balayage et Microanalyses, EDP Sciences, Paris, 2009, ISBN 978-2-7598-0082-7.
[43] A. Dessombz, P. Méria, D. Bazin, M. Daudon, PLoS One 7 (2012) e51691.
[44] M. Daudon, P. Jungers, D. Bazin, N. Engl. J. Med. 359 (2008) 100.
[45] J.L. Pariente, P. Conort, Prog. Urol. 1 (2005) 897.
[46] M. Rubinstein, R.H. Colby, Polymer Physics, Oxford University Press, Oxford, 2003, ISBN 9780198520597.
[47] L. Estepa, M. Daudon, Biospectroscopy 3 (1997) 347.
[48] N. Quy Dao, M. Daudon, Infrared and Raman Spectra of calculi, Elsevier, Paris, 1997.
[49] M. Daudon, O. Traxer, B. Doré, H. Hadjadj, P. Conort, members of the Comité Lithiase de l'Association Française d'Urologie, Sémin. Urol. Néphrol. 31 (2005) 186.
[50] E. Letavernier, O. Traxer, J.P. Haymann, D. Bazin, M. Daudon, Prog. Urol. FMC 22 (2012) F119.
[51] D. Bazin, M. Daudon, G. André, R. Weil, E. Véron, G. Matzen, J. Appl. Crystallogr. 47 (2014) 719.
[52] M. Livrozet, S. Vandermeersch, L. Mesnard, E. Thioulouse, J. Jaubert, J.-J. Boffa, J.-P. Haymann, L. Baud, D. Bazin, M. Daudon, E. Letavernier, PLoS One 9 (2014) e102700.
[53] M. Van Meerssche, J. Feneau-Dupont, Introduction à la Cristallographie et à la Chimie Structurale, Vander, Louvain, Belgium, 1973.
[54] J. Prywer, A. Torzewska, T. Płociński, Urol. Res. 40 (2012) 699.
[55] D. Bazin, G. André, R. Weil, G. Matzen, E. Véron, M. Daudon, Urology 79 (2012) 786.
[56] R. Flannigan, W.H. Choy, B. Chew, D. Lange, Nat. Rev. Urol. 11 (2014) 333.
[57] X. Carpentier, M. Daudon, O. Traxer, P. Jungers, A. Mazouyes, G. Matzen, E. Véron, D. Bazin, Urology 73 (2009) 968.
[58] K.M. Englert, J.A. McAteer, J.E. Lingeman, J.C. Williams Jr., Urolithiasis 41 (2013) 389.